Frontiers of Physics
https://doi.org/10.1007/s11467-021-1066-9
Front. Phys.
16(5), 53506 (2021)

RESEARCH ARTICLE

A DFT study of $Ti_3C_2O_2$ MXenes quantum dots supported on single layer graphene: Electronic structure and hydrogen evolution performance

Qingquan Kong[1], Xuguang An[1], Lin Huang[1], Xiaolian Wang[1], Wei Feng[1], Siyao Qiu[2], Qingyuan Wang[1,†], Chenghua Sun[2,3,‡]

[1] *School of Mechanical Engineering, Chengdu University, Chengdu 610106, China*
[2] *College of Chemical Engineering and Energy Technology, Dongguan University of Technology, Dongguan 523808, China*
[3] *Department of Chemistry and Biotechnology, and Center for Translational Atomaterials, Swinburne University of Technology, Hawthorn, VIC 3122, Australia*
Corresponding authors. E-mail: [†] *wangqy@cdu.edu.cn,* [‡] *chenghuasun@swin.edu.au*
Received September 21, 2020; accepted January 4, 2021

Heterojunction structure has been extensively employed for the design of novel catalysts. In the present study, density functional theory was utilized to investigate the electronic structure and hydrogen evolution performance of $Ti_3C_2O_2$ MXene quantum dots/graphene (QDs/G) heterostructure. Results show that a slight distortion can be observed in graphene after hybriding with QDs, due to which the electronic structure of QDs have been changed. Associated with such QDs-graphene interaction, the catalytic activity of $Ti_3C_2O_2$ QDs has been optimized, leading to excellent HER catalytic performance.

Keywords MXenes, quantum dots, density functional theory (DFT), hydrogen evolution reaction (HER)

1 Introduction

Hydrogen energy is a clean and sustainable energy, which can be a promising alternative for carbon-based fuels [1]. Hydrogen evolution reaction (HER) in elctrocatalytic water splitting has the advantage of effectively producing high purity hydrogen in comparison with natural gas reforming [2], without raising any carbon emission. Development of high performance electrocatalysts to overcome the drawbacks such as high overpotential and low efficiency is highly demanded [3–5]. So far, the most active catalysts for the HER are precious metals such as platinum (Pt), palladium (Pd) and other noble metal materials [6–8]. Unfortunately, the scarcity of noble metals has hindered their large-scale industrial applications. Therefore, the development of non-precious electrocatalysts with high catalytic activity and stability is necessary.

Recently, MXenes with OH, O, and F terminated functional groups have aroused remarkable attention owing to their excellent electrical conductivity, chemical stability and abundant active catalytic sites [9, 10]; as a result, MXenes have emerged as a novel family and been extensively employed for various photo/electrochemical applications, such as HER [11–15], nitrogen reduction reaction (NRR) [16], CO_2 reduction reaction (CO_2RR) [17], and battery [18]. The chemical formula of MXenes can be expressed as $M_{n+1}X_nT_x$ (n = 1, 2 and 3), where M stands for the transition metal, X represents the nitrogen or carbon or carbonitride, and T_x represents surface functional groups. Wang *et al.* firstly predicted the high HER activity of transition metal-promoted V_2CO_2 [11]. Then a comprehensive work combined theoretical and experimental study showed Mo_2CT_x exhibit high HER activity as well as stability [12]. Following that, several groups were dedicated to exploring more possible candidates for HER catalyst among MXenes [13, 19–26], focusing on MXene nanosheets and modifications. To further improve the performance, MXenes with zero-dimension (0D), also known as quantum dots (QDs), have been explored given QDs offer abundant active edging sites. Photocatalytic CO_2 conversion ability of Cu_2O nanowires can be enhanced by MXene QDs [27]. Titanium carbide MXene QDs with high near-infrared photothermal performances also studied for cancer therapy [28]. Recently, hydroxyl-rich $Ti_3C_2T_x$ MXene QDs have been rationally designed and synthesized for electrochemical N_2 reduction [29]. MXene QDs can also be a good catalyst for HER, however, it is rarely reported.

Inspired by these researches, we aimed to explore MXene QDs as electrocatalysts for HER. Different from 2D nanosheets, QDs prefer to aggregate if no constraint is applied, which will remarkably reduce active sites and increase phase/interface resistance. Therefore, QDs have to

*Special Topic: Heterojunction and Its Applications (Ed. Chenghua Sun). This article can also be found at http://journal.hep.com.cn/fop/EN/10.1007/s11467-021-1066-9.

© Higher Education Press 2021

be smartly loaded on catalysts support, which can offer large surface area, high conductivity and strong capacity to fix QDs [30]. So far, however, the knowledge regarding the interaction between MXene QDs and the substrate is quite limited. Most recently, g-C_3N_4@Ti_3C_2 QDs were reported as an efficient co-catalyst for photocatalytic H_2 production, which primarily ascribed to the fast photoexcited electrons transferring phenomenon between Ti_3C_2 QDs and g-C_3N_4 [31]. 2D/2D/0D TiO_2/C_3N_4/Ti_3C_2 MXene composite was also demonstrated with excellent CO_2 reduction activity [32]. As stated in the literature, low-dimensional materials often show quite different properties from their parent ones [33–36]. Therefore, a fundamental question would be what will happen when two components with different dimensions are mixed to form a heterojunction.

In this study, we put such general question in the context of HER catalysis as this reaction is two-electron process, whose mechanism has been extensively studied. In our case, catalyst design starts from $Ti_3C_2O_2$ MXene QDs as 0D component, which is loaded to graphene (G) to generate a concept material, 0D/2D hybrid structure. Graphene and $Ti_3C_2O_2$ MXene QDs are employed because both have been synthesized readily in the lab, and have been demonstrated as excellent functional materials for a lot of applications [37–39]. Our interest is to clarify the interaction between MXene QDs and graphene, focusing on the electron transfer between two components and its effect on the hydrogen evolution performance.

2 Computational methods

First-principles calculations were performed using Vienna ab initio simulation package (VASP) within the framework of density functional theory (DFT) [40]. Projector Augmented Wave (PAW) was used to describe the interaction between valence electrons and ionic core [41]. Generalized gradient approximation (GGA) with the revised Perdew–Burke–Ernzerhof functional (RPBE) was adopted to describe exchange-correlation functional effect [42]. Plane wave basis functions were expanded with a cutoff energy of 450 eV. K-points were sampled using 6×6×1 Gamma mesh for density of states (DOS) and 3 ×3 ×1 for the structural optimization, respectively. The thickness of the vacuum region is >15 Å to avoid the spurious interaction. All of the structures are optimized until the forces exerted on each atom are less than 0.03 eV/Å and the total energy less than 10^{-5} eV. The van der Waals interaction between non-bonding atoms was described by empirical DFT-D3 [43, 44]. Hybrid functional method (HSE06) was adopted to calculate the band structures [45]. Crystal orbital Hamilton population (COHP) analysis was performed by *LOBSTER* software [46, 47].

For HER calculations, Gibbs free energy of the intermediate hydrogen adsorbed on the catalyst (ΔG_{H^*}) is critical to evaluate the catalyst activity [13, 48]. G_{H^*} can be expressed as

$$G_{H^*} = \Delta E_{H^*} + \Delta E_{ZPE} - T\Delta S_H,$$

where ΔE_{H^*} is the adsorption energy of atomic hydrogens on the given unit cell, ΔE_{ZPE} is the difference corresponding to the zero point energy between the adsorbed hydrogen and hydrogen in the gas phase, and ΔS_H is entropy change associated with H* adsorption. The exchange current at pH = 0 can be calculated based on Nørskov's assumption as follows [48]:

$$i_0 = -ek_0 \frac{1}{1+\exp(-\frac{\Delta G_{H^*}}{kT})} \quad \text{for} \quad G_{H^*} < 0,$$

$$i_0 = -ek_0 \frac{1}{1+\exp(-\frac{\Delta G_{H^*}}{kT})} \exp(-\frac{\Delta G_{H^*}}{kT}) \quad \text{for } \Delta G_{H^*} > 0,$$

where k_0 is the rate constant, which equals to 200 s^{-1}/site.

3 Results and discussion

MXene quantum dots (QDs) offer large amount of surface defects and high surface specific area, generating abundant active basal and edge sites, which can be used as high performance electrocatalysts and photocatalysts [29, 31]. Generally, MXenes terminated by oxygen atom are thermodynamically preferred [21, 49]. As a typical 2D materials, graphene exhibits excellent electrical conductivity and extremely high specific surface area; moreover, it has been extensively explored as a support material to improve electrocatalytic activity [50–53]. Specially, oxygen functionalized $Ti_3C_2T_x$ MXene shows enhanced HER properties [26]. Therefore, Ti_3C_2 QDs with O surface functional groups and graphene were employed to form a heterojunction in this study. After the relaxation of graphene, we find that the interatomic distance between carbon atoms is 0.142 nm and the angle is ~120°, which is consistent with previous study [22]. Figure 1 shows the lattice structure of QDs/G heterostructure after structural optimization. Compared with initial structure, a slight distortion

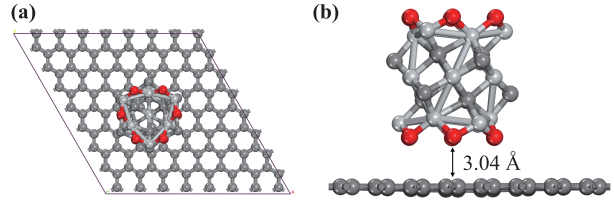


Fig. 1 Computational model for Ti_3C_2 QDs/G heterostructure. Top view **(a)** and side view **(b)** with carbon, oxygen and titanium atoms shown as by dark gray, red and light gray balls. The distance between QDs and graphene substrate is indicated.

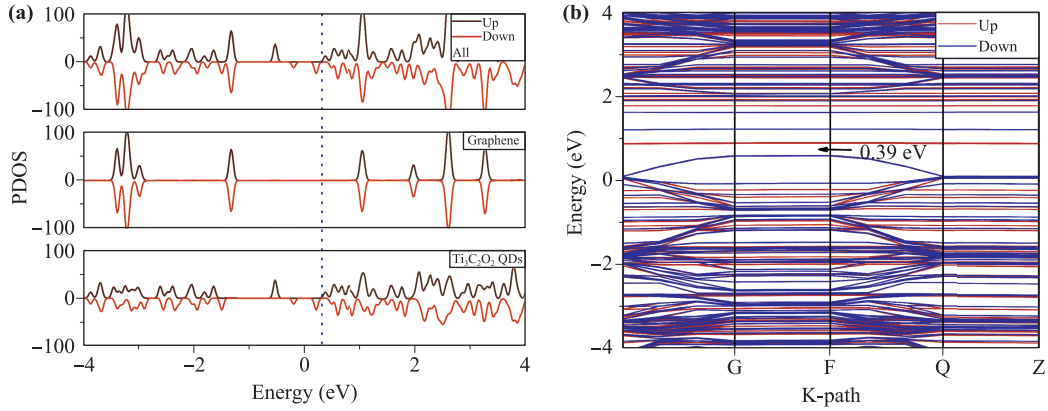


Fig. 2 Calculated electronic structures of $Ti_3C_2O_2$ QDs/G heterostructure. **(a)** PDOS profiles for total, QDs and graphene; and **(b)** band structure. Fermi levels are set at 0 eV.

phenomenon can be observed in graphene after decorated with QDs. Moreover, adsorption energy of $Ti_3C_2O_2$ QDs on graphene is −0.71 eV, indicating that QDs can be effectively adsorbed by graphene, but the interfacial interaction is not as strong as chemical bonding, being consistent with calculated QD-graphene distance (3.04 Å, see Fig. 1).

Then we turn to the electronic structure of QDs/G heterostructure. Projected density of states (PDOS) profiles of graphene and $Ti_3C_2O_2$ QDs are shown in Fig. S1, respectively. Graphene shows the classic zero-gap feature, in good agreement with previous theoretical studies [54]. Band structure of graphene has been shown in Fig. S2, also supporting the above results. Xie *et al.* reported that $Ti_{n+1}C_nO_2$ is metallic except for Ti_2CO_2 [55]. Both surface terminations, size, and orientation can influence MXenes' electronic structure [56]. As shown in Fig. S1(b), Ti_3C_2 QDs also show metallic features, which are beneficial for electrocatalysis like HER as studied here. For surface catalysis, electronic states being around Fermi level often play the key role during the reactions [55]. For Ti_3C_2 QDs, DOS at E_F is much higher than the ideal 2D nanosheet [55], which can be attributed to the nano-size effect, such as dangling bonds. PDOS and band structure for Ti_3C_2 QDs/G heterostructure are shown in Figs. 2(a) and (b), showing a band gap of 0.39 eV. Thus, the electronic structure of graphene has been tuned by quantum dots (band gap opening), which might open a new window to develop high-tech 2D electronic devices.

In order to analyze the charge transfer between these two components, differential charge was calculated, together with Bader charge analysis. As demonstrated below, both differential charge and Bader analysis results confirm that the interaction between these two components is essentially weak van der Waals interaction and polarization, being consistent with QD adsorption energy shown above (−0.71 eV). Figure 3(a) shows differential charge density of $Ti_3C_2O_2$ QDs/G heterostructure, where the yellow and cyan represent electron accumulation and depletion, respectively. Accordingly, O-terminals in QDs bring strong local electron accumulation, showing as negatively charge center, which can change the homogeneous π-bonding on graphene basal plane. As a result, electron depletion area has been found (cyan), being surrounded by negatively charged regions. As a result, only small amount of electrons has been transferred between two components, as demonstrated by Bader charge of δ(graphene)≈0 and δ(MXene QD) ≈ 0. Such heterojunction nature can be further vividly shown by calculated Electron Localization Function [ELF, see Fig. 3(b)], in which almost no direct bonding between graphene and QD is presented. Therefore, the QD/graphene interaction is dominated by interfacial polarization.

Given QDs present non-bonding states (from lowly coordinated oxygen), which can result in severe interfacial polarization, it is worthy to further examine the C–O interaction over the interface. Crystal orbital Hamilton population (COHP) method is a useful tool to visualize and analyze chemical bonding [57]. To understand the origin of the distortion of graphene after $Ti_3C_2O_2$ QDs modification, the COHP curves were examined. As shown in Fig. 4(a), significant antibonding C–O interactions at Fermi level for initial configuration can be observed, re-

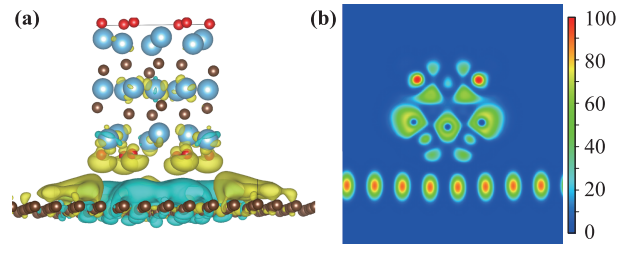


Fig. 3 Charge analysis. **(a)** Charge density difference for $Ti_3C_2O_2$ QDs/G heterostructure, with an isosurfaces beings set to 0.0002 e/Å^3 in positive and negative mode, where the yellow and cyan represent electron accumulation and depletion, respectively, **(b)** ELF images for $Ti_3C_2O_2$ QDs/G heterostructure.

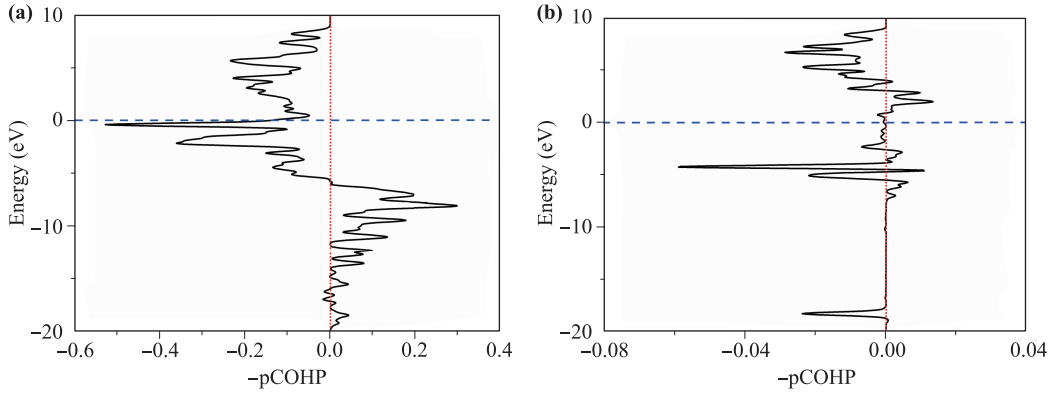


Fig. 4 O–C bond analysis using –pCOHP curve for $Ti_3C_2O_2$ QDs/G heterostructure. Calculated –pCOHP profiles with **(a)** before and **(b)** after structure optimization. The Fermi level is represented by the blue dash line. Positive and negative –pCOHP indicate the bonding and antibonding states.

vealing that the configuration is not stable, which is the driving force for QDs aggregation. According to Dronskowski's researches, stable configuration can be obtained through introducing vacancy or structural transformation, etc. [57]. As revealed in Fig. 4(b), graphene was twisted, and the antibonding state of its COHP disappears at Fermi level, indicating a stabilization due to QD-graphene interaction. Combining with calculated charge density difference, ELF and COHP, it is concluded that the electronically unfavorable situation for QDs and graphene can be improved by the distortion of graphene, which leads to the electron redistribution and electronic structure change.

Following the above analysis, it is worth investigating what kind of effect will be generated for catalysis performance. In our case, HER has been employed as a model reaction for this purpose. Initially, the HER activity of both $Ti_3C_2O_2$ QDs and heterostructure under standard conditions are investigated. The vertical view and side

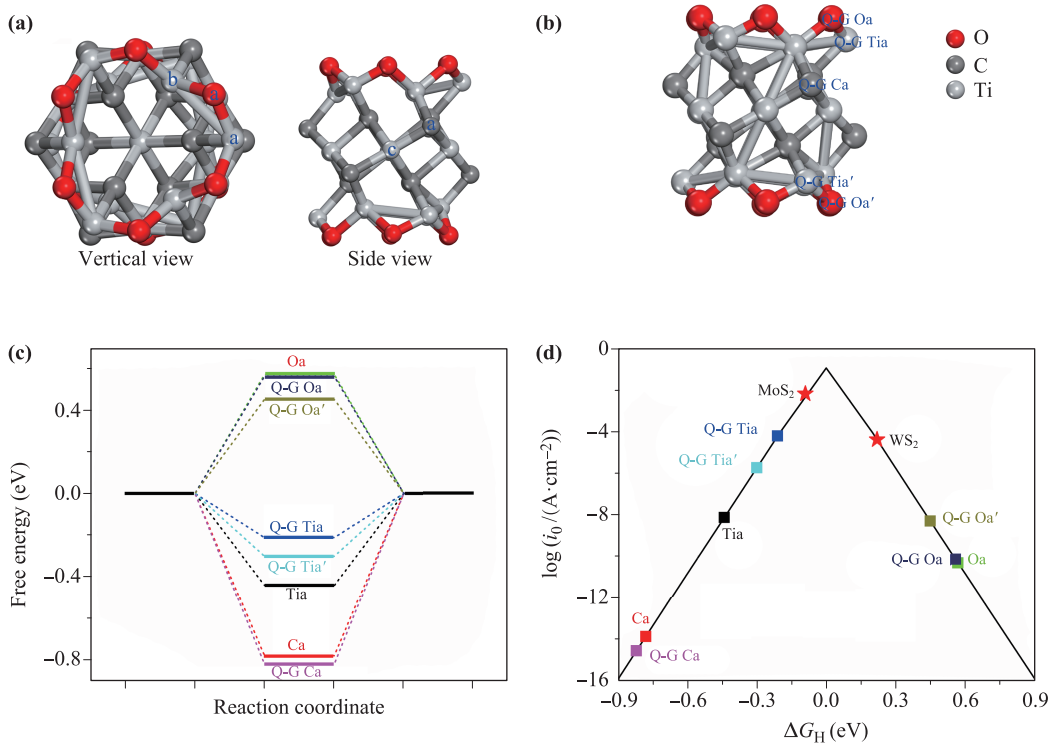


Fig. 5 HER performance of $Ti_3C_2O_2$ QDs and QDs/G heterostructure. **(a)** H* adsorption sites of $Ti_3C_2O_2$ QDs, **(b)** H* adsorption sites of $Ti_3C_2O_2$ QDs/G heterostructure, **(c)** free energy diagram of HER processing on different site of $Ti_3C_2O_2$ QDs and QDs/G heterostructure and **(d)** volcano curve of exchange current (i_0) as a function of the Gibbs free energy of hydrogen adsorption ΔG_H. The subscript a and b in Tia, Tib, Oa and Ob are labelled in (a).

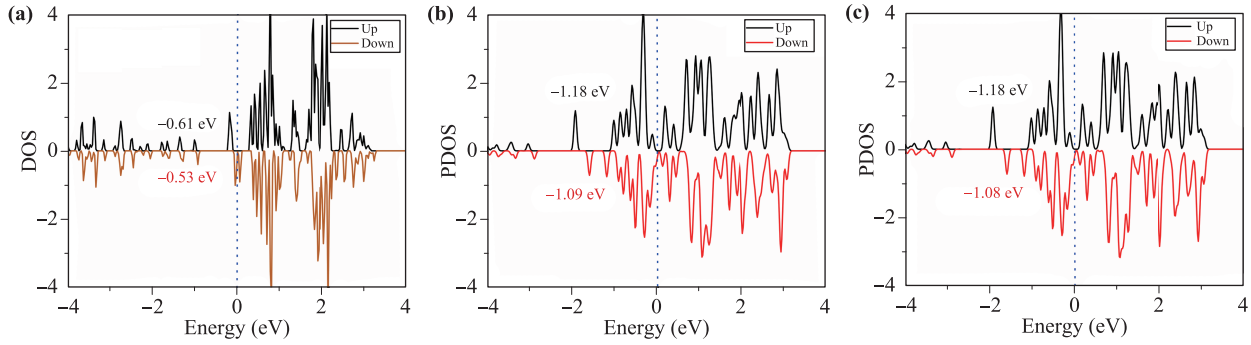


Fig. 6 Calculated PDOS for Ti for **(a)** $Ti_3C_2O_2$ QDs, **(b)** Tia and **(c)** Tia′ sites for $Ti_3C_2O_2$ QDs/G heterostructure. Fermi levels are set at 0 eV. Calculated d-band center for spin-up (black) and spin-down (red) are labelled in the figure, respectively.

view of $Ti_3C_2O_2$ QDs are shown in Fig. 5(a). Gibbs free energy of H* adsorption (ΔG_H) on various sites of QDs, such as Oa, Tia, Tib, Tic and Ca [labelled in Fig. 5(a)], was calculated. Tia, Ca and Oa can be remained after structural optimization. During the optimization, H absorbed on Tic site prefers to move to Oa site, and H absorbed on Tib site also moves to Ca site, as demonstrated by the energy change during geometry optimization (see Fig. S3). Based on optimized geometries for H-adsorption, calculated values of ΔG_H for Tia, Ca and Oa sites are −0.44, −0.78 and 0.57 eV, respectively. A key difference is that Ti-site is more favorable for H-adsorption, rather than O-site as reported with ideal 2D MXenes [26]. For $Ti_3C_2O_2$ QDs/G heterostructure, ΔG_H of Tia site is −0.21 eV, indicating that it is potentially an excellent catalyst for the HER. It is worth noting that the E_{ZPE} of adsorbed state for all the systems obtained by vibrational frequency calculation are quite different (Table S1). E_{ZPE} for O adsorption site is same as previous study that about 0.30 eV [13, 19]. However, E_{ZPE} for Ti sites are slightly smaller due to the fact that H is negatively charged in H–Ti interaction, essentially different from that in the H–O case as presented in ideal 2D MXene layers [13, 19].

To further compare the HER performance for different active sites of studied materials, a volcano curve is plotted, MoS_2 and WS_2 are supplied for comparison [Fig. 5(d)]. HER performance can be quantitatively evaluated by the position of its i_0 and ΔG_H values. The superior HER catalysis properties can be obtained near the volcano peak. The interactions of adsorbed H and Ca sites are too strong with a large negative ΔG_H of less than −0.70 eV, demonstrating a low exchange current. ΔG_H of Oa sites for QDs and QDs/G heterostructure are 0.4–0.6 eV, which is different from 2D $Ti_3C_2O_2$ MXenes [13, 58]. As a contrast, Tia site has been identified as the most suitable side for HER catalysis, with $\Delta G_H = -0.44$ eV. Now we turn to the QDs/Graphene heterojunction case. As shown in Fig. 5(b), ΔG_H over Ti-site is down to −0.21 eV (Tia) and −0.30 eV (Tia′), both performing better than that obtained from pure QDs. To understand this, Fig. 6 compares d-orbital PDOS of Tia- and Tia′-site for QDs and QDs/G heterostructure, with d-band centre being labelled in unit of eV. Clearly, the d band center shifts towards the deep-energy level by 0.4–0.5 eV due to the hybriding with graphene support, which is beneficial to obtain preferable H adsorb energy because the issue for QDs is that H–Ti interaction is too strong [59, 60]. As a result, superior HER properties can be achieved from this MXene QDs/Graphene heterojunction.

4 Conclusions

In conclusion, we proposed QDs/graphene heterojunction as a model 0D/2D catalyst and investigated the electronic interaction between QDs and graphene. It is demonstrated that the interaction is dominated by interfacial polarization, instead of chemical bonding. As a result, slight distortion can be observed in graphene after being decorated with QDs, which can be utilized to tune the electronic structure of QDs and graphene. Due to the zero-dimension feature and interfacial interaction, $Ti_3C_2O_2$ QDs/graphene shows excellent HER performance with ΔG_H of −0.21 eV. Following this prediction, it is expected that 0D/2D heterojunctions, or more general multiple dimension designs, offer large space for rational design of catalysts. Ongoing work is being under progress to further improve HER performance by optimizing MXens QDs with proper composition or/and computationally screening a variety of catalyst supports such as g-C_3N_4 and phosphine.

Electronic supplementary material Electronic supplementary materials are available in the online version of this article at https://doi.org/10.1007/s11467-021-1066-9 and http://journal.hep.com.cn/fop/EN/10.1007/s11467-021-1066-9 are accessible for authorized users.

Acknowledgements The authors would like to acknowledge funding from the National Natural Science Foundation of China

(Grant No. 11832007), China Postdoctoral Science Foundation (Grant No. 2018M631082), Application and Foundation Research Projects of Sichuan Province (Grant Nos. 2018JY0062 and 2019YJ0668), Guangdong Innovation Research Team for Higher Education (Grant No. 2017KCXTD030), High-level Talents Project of Dongguan University of Technology (Grant No. KCYKYQD2017017). The authors also thank Ming Yan from China Three Gorges University for HSE BAND calculations.

References

1. J. A. Turner, Sustainable hydrogen production, *Science* 305(5686), 972 (2004)
2. S. Bhavsar, M. Najera, R. Solunke, and G. Veser, Chemical looping: To combustion and beyond, *Catal. Today* 228(0), 22896 (2014)
3. P. Li, R. Zhao, H. Chen, H. Wang, P. Wei, H. Huang, Q. Liu, T. Li, X. Shi, Y. Zhang, M. Liu, and X. Sun, Recent advances in the development of water oxidation electrocatalysts at mild pH, *Small* 15(13), 1805103 (2019)
4. D. Li, J. Shi, and C. Li, Transition-metal-based electrocatalysts as cocatalysts for photoelectrochemical water splitting: A mini review, *Small* 14(23), 1704179 (2018)
5. S. Wang, P. Chen, Y. Bai, J. H. Yun, G. Liu, and L. Wang, New $BiVO_4$ dual photoanodes with enriched oxygen vacancies for efficient solar-driven water splitting, *Adv. Mater.* 30(20), 1800486 (2018)
6. Y. Zheng, Y. Jiao, M. Jaroniec, and S. Z. Qiao, Advancing the electrochemistry of the hydrogen-evolution reaction through combining experiment and theory, *Angew. Chem. Int. Ed.* 54(1), 52 (2015)
7. A. Eftekhari, Electrocatalysts for hydrogen evolution reaction, *Int. J. Hydrogen Energy* 42(16), 11053 (2017)
8. Z. Tang, S. Shen, J. Zhuang, and X. Wang, Noble-metal-promoted three-dimensional macroassembly of single-layered graphene oxide, *Angew. Chem. Int. Ed.* 49(27), 4603 (2010)
9. M. Naguib, V. N. Mochalin, M. W. Barsoum, and Y. Gogotsi, MXenes: A new family of two-dimensional materials, *Adv. Mater.* 26(7), 992 (2014)
10. J. C. Lei, X. Zhang, and Z. Zhou, Recent advances in MXene: Preparation, properties, and applications, *Front. Phys.* 10(3), 276 (2015)
11. Z. W. Seh, K. D. Fredrickson, B. Anasori, J. Kibsgaard, A. L. Strickler, M. R. Lukatskaya, Y. Gogotsi, T. F. Jaramillo, and A. Vojvodic, Two-dimensional molybdenum carbide (MXene) as an efficient electrocatalyst for hydrogen evolution, *ACS Energy Lett.* 1(3), 589 (2016)
12. G. Gao, A. P. O' Mullane, and A. Du, 2D MXenes: A new family of promising catalysts for the hydrogen evolution reaction, *ACS Catal.* 7(1), 494 (2017)
13. Y. Li, Z. Yin, G. Ji, Z. Liang, Ya. Xue, Y. Guo, J. Tian, X. Wang, and H. Cui, 2D/2D/2D heterojunction of Ti_3C_2 MXene/MoS_2 nanosheets/TiO_2 nanosheets with exposed (001) facets toward enhanced photocatalytic hydrogen production activity, *Appl. Catal. B* 246(5), 12 (2019)
14. Y. Li, L. Ding, S. Yin, Z. Liang, Y. Xue, X. Wang, H. Cui, and J. Tian, Photocatalytic H_2 evolution on TiO_2 assembled with Ti_3C_2 MXene and metallic 1T WS_2 as Co catalysts, *Nano-Micro Lett.* 12(1), 6 (2020)
15. Y. Li, L. Ding, Z. Liang, Y. Xue, H. Cui, and J. Tian, Synergetic effect of defects rich MoS_2 and Ti_3C_2 MXene as cocatalysts for enhanced photocatalytic H_2 production activity of TiO_2, *Chem. Eng. J.* 383(1), 123178 (2020)
16. L. M. Azofra, N. Li, D. R. MacFarlane, and C. Sun, Promising prospects for 2D d2-d4 M_3C_2 transition metal carbides (MXenes) in N_2 capture and conversion into ammonia, *Energy Environ. Sci.* 9(8), 2545 (2016)
17. N. Li, X. Chen, W. J. Ong, D. R. MacFarlane, X. Zhao, A. K. Cheetham, and C. Sun, Understanding of electrochemical mechanisms for CO_2 capture and conversion into hydrocarbon fuels in transition-metal carbides (MXenes), *ACS Nano* 11(11), 10825 (2017)
18. X. Chen, Z. Kong, N. Li, X. Zhao, and C. Sun, Proposing the prospects of Ti_3CN transition metal carbides (MXenes) as anodes of Li-ion batteries: A DFT study, *Phys. Chem. Chem. Phys.* 18(48), 32937 (2016)
19. C. Ling, L. Shi, Y. Ouyang, and J. Wang, Searching for highly active catalysts for hydrogen evolution reaction based on O-terminated MXenes through a simple descriptor, *Chem. Mater.* 28(24), 9026 (2016)
20. Z. Guo, Z. Jian, and Z. Sun, New two-dimensional transition metal borides for Li ion battery and electrocatalysis, *J. Mater. Chem. A* 5(45), 23530 (2017)
21. M. Pandey and K. S. Thygesen, Two-dimensional MXenes as catalysts for electrochemical hydrogen evolution: A computational screening study, *J. Phys. Chem. C* 121(25), 13593 (2017)
22. Y. W. Cheng, J. H. Dai, Y. M. Zhang, and Y. Song, Two-dimensional, ordered, double transition metal carbides (MXenes): A new family of promising catalysts for the hydrogen evolution reaction, *J. Phys. Chem. C* 122(49), 28113 (2018)
23. B. Huang, N. Zhou, X. Chen, W. J. Ong, and N. Li, Insights into the electrocatalytic hydrogen evolution reaction mechanism on two-dimensional transition-metal carbonitrides (MXene), *Chemistry* 24(69), 18479 (2018)
24. H. Zhang, L. Yu, T. Chen, W. Zhou, and X. W. D. Lou, Surface modulation of hierarchical MoS_2 nanosheets by Ni single atoms for enhanced electrocatalytic hydrogen evolution, *Adv. Funct. Mater.* 28(51), 1807086 (2018)
25. Y. Cheng, L. Wang, Y. Song, and Y. Zhang, Deep insights into the exfoliation properties of MAX to MXenes and the hydrogen evolution performances of 2D MXenes, *J. Mater. Chem. A* 7(26), 15862 (2019)
26. Y. Jiang, T. Sun, X. Xie, W. Jiang, J. Li, B. Tian, and C. Su, Oxygen-functionalized ultrathin $Ti_3C_2T_x$ MXene for enhanced electrocatalytic hydrogen evolution, *ChemSusChem* 12(7), 1368 (2019)
27. Z. Zeng, Y. Yan, J. Chen, P. Zan, Q. Tian, and P. Chen, Boosting the photocatalytic ability of Cu_2O nanowires for CO_2 conversion by MXene quantum dots, *Adv. Funct. Mater.* 29(2), 1806500 (2019)

28. X. Yu, X. Cai, H. Cui, S. W. Lee, X. F. Yu, and B. Liu, Fluorine-free preparation of titanium carbide MXene quantum dots with high near-infrared photothermal performances for cancer therapy, *Nanoscale* 9(45), 17859 (2017)
29. Z. Jin, C. Liu, Z. Liu, J. Han, Y. Fang, Y. Han, Y. Niu, Y. Wu, C. Sun, and Y. Xu, Rational design of hydroxyl-rich $Ti_3C_2T_x$ MXene quantum dots for high-performance electrochemical N_2 reduction, *Adv. Energy Mater.* 10(22), 2000797 (2020)
30. C. Tsai, F. Abild-Pedersen, and J. K. Nørskov, Tuning the MoS_2 edge-site activity for hydrogen evolution via support interactions, *Nano Lett.* 14(3), 1381 (2014)
31. Y. Li, L. Ding, Y. Guo, Z. Liang, H. Cui, and J. Tian, Boosting the photocatalytic ability of g-C_3N_4 for hydrogen production by Ti_3C_2 MXene quantum dots, *Acs Appl. Mater. Inter.* 11(44), 41440 (2019)
32. F. He, B. Zhu, B. Cheng, J. Yu, W. Ho, W. Macyk, 2D/2D/0D $TiO_2/C_3N_4/Ti_3C_2$ MXene composite S-scheme photocatalyst with enhanced CO_2 reduction activity, *Applied Catalysis B* 272(0), 119006(2020)
33. Z. Cui, W. Du, C. Xiao, Q. Li, R. Sa, C. Sun, and Z. Ma, Enhancing hydrogen evolution of MoS_2 Basal planes by combining single-boron catalyst and compressive strain, *Front. Phys.* 15(6), 63502 (2020)
34. Q. Yu, Y. Luo, S. Qiu, Q. Li, Z. Cai, Z. Zhang, J. Liu, C. Sun, and B. Liu, Tuning the hydrogen evolution performance of metallic 2D tantalum disulfide by interfacial engineering, *ACS Nano* 13(10), 11874 (2019)
35. K. Chu, Y. Liu, Y. Li, H. Zhang, and Y. Tian, Efficient electrocatalytic N_2 reduction on CoO quantum dots, *J. Mater. Chem. A* 7(9), 4389 (2019)
36. H. Liu, X. Zhang, Y. Zhu, B. Cao, Q. Zhu, P. Zhang, B. Xu, F. Wu, and R. Chen, Electrostatic self-assembly of 0D–2D SnO_2 quantum dots/$Ti_3C_2T_x$ MXene hybrids as anode for lithium-ion batteries, *Nano-Micro Lett.* 11(1), 65 (2019)
37. X. Chen, X. Sun, W. Xu, G. Pan, D. Zhou, J. Zhu, H. Wang, X. Bai, B. Dong, and H. Song, Ratiometric photoluminescence sensing based on Ti_3C_2 MXene quantum dots as an intracellular pH sensor, *Nanoscale* 10(3), 1111 (2018)
38. Y. Qin, Z. Wang, N. Liu, Y. Sun, D. Han, Y. Liu, L. Niu, and Z. Kang, High-yield fabrication of $Ti_3C_2T_x$ MXene quantum dots and their electrochemiluminescence behavior, *Nanoscale* 10(29), 14000 (2018)
39. Q. Xu, L. Ding, Y. Wen, W. Yang, H. Zhou, X. Chen, J. Street, A. Zhou, W. J. Ong, and N. Li, High photoluminescence quantum yield of 18.7% by using nitrogen-doped Ti_3C_2 MXene quantum dots, *J. Mater. Chem. C* 6(24), 6360 (2018)
40. G. Kresse and J. Furthmüller, Efficient iterative schemes for *ab initio* total-energy calculations using a plane-wave basis set, *Phys. Rev. B* 54(16), 11169 (1996)
41. P. E. Blöchl, Projector augmented-wave method, *Phys. Rev. B* 50(24), 17953 (1994)
42. J. P. Perdew, K. Burke, and Y. Wang, Generalized gradient approximation for the exchange-correlation hole of a many-electron system, *Phys. Rev. B* 54(23), 16533 (1996)
43. S. Grimme, Accurate description of van der Waals complexes by density functional theory including empirical corrections, *J. Comput. Chem.* 25(12), 1463 (2004)
44. S. Grimme, Semiempirical GGA-type density functional constructed with a long-range dispersion correction, *J. Comput. Chem.* 27(15), 1787 (2006)
45. J. Heyd, G. E. Scuseria, and M. Ernzerhof, Hybrid functionals based on a screened Coulomb potential, *J. Chem. Phys.* 118(18), 8207 (2003)
46. V. L. Deringer, A. L. Tchougréeff, and R. Dronskowski, Crystal orbital Hamilton population (COHP) analysis as projected from plane-wave basis sets, *J. Phys. Chem. A* 115(21), 5461 (2011)
47. S. Maintz, V. L. Deringer, A. L. Tchougréeff, and R. Dronskowski, LOBSTER: A tool to extract chemical bonding from plane-wave based DFT, *J. Comput. Chem.* 37(11), 1030 (2016)
48. J. K. Nørskov, T. Bligaard, A. Logadottir, J. R. Kitchin, J. G. Chen, S. Pandelov, and U. Stimming, Trends in the exchange current for hydrogen evolution, *J. Electrochem. Soc.* 152(3), J23 (2005)
49. Z. Shen, X. Fan, S. Ma, Y. An, D. Yang, N. Guo, Z. Luo, and Y. Hu, 3d transitional-metal single atom catalysis toward hydrogen evolution reaction on MXenes supports, *Int. J. Hydrogen Energy* 45(28), 14396 (2020)
50. L. Dong, R. R. S. Gari, Z. Li, M. M. Craig, and S. Hou, Graphene-supported platinum and platinum–ruthenium nanoparticles with high electrocatalytic activity for methanol and ethanol oxidation, *Carbon* 48(3), 781 (2010)
51. Y. Li, H. Wang, L. Xie, Y. Liang, G. Hong, and H. Dai, MoS_2 nanoparticles grown on graphene: An advanced catalyst for the hydrogen evolution reaction, *J. Am. Chem. Soc.* 133(19), 7296 (2011)
52. K. Chu, Y. Liu, J. Wang, and H. Zhang, NiO nanodots on graphene for efficient electrochemical N_2 reduction to NH_3, *ACS Appl. Energy Mater.* 2(3), 2288 (2019)
53. X. Zhang, Q. Liu, X. Shi, A. M. Asiri, Y. Luo, X. Sun, and T. Li, TiO_2 nanoparticles–reduced graphene oxide hybrid: An efficient and durable electrocatalyst toward artificial N_2 fixation to NH_3 under ambient conditions, *J. Mater. Chem. A* 6(36), 17303 (2018)
54. L. B. Drissi, E. H. Saidi, M. Bousmina, and O. Fassi-Fehri, DFT investigations of the hydrogenation effect on silicene/graphene hybrids, *J. Phys.: Condens. Matter* 24(48), 485502 (2012)
55. Y. Xie and P. Kent, Hybrid density functional study of structural and electronic properties of functionalized $Ti_{n+1}X_n$ (X=C, N) monolayers, *Phys. Rev. B* 87(23), (2013)
56. M. Naguib, M. Kurtoglu, V. Presser, J. Lu, J. Niu, M. Heon, L. Hultman, Y. Gogotsi, and M. W. Barsoum, Two-dimensional nanocrystals produced by exfoliation of Ti_3AlC_2, *Adv. Mater.* 23(37), 4248 (2011)
57. S. Steinberg and R. Dronskowski, The crystal orbital Hamilton population (COHP) method as a tool to visualize and analyze chemical bonding in intermetallic compounds, *Crystals (Basel)* 8(5), 225 (2018)

58. J. Ran, G. Gao, F. T. Li, T. Y. Ma, A. Du, and S. Z. Qiao, Ti_3C_2 MXene co-catalyst on metal sulfide photo-absorbers for enhanced visible-light photocatalytic hydrogen production, *Nat. Commun.* 8(1), 13907 (2017)

59. Q. Liu, H. Zhao, M. Jiang, Q. Kang, W. Zhou, P. Wang, and F. Zhou, Boron enhances oxygen evolution reaction activity over Ni foam-supported iron boride nanowires, *J. Mater. Chem. A* 8(27), 13638 (2020)

60. X. Luo, Q. Shao, Y. Pi, and X. Huang, Trimetallic molybdate nanobelts as active and stable electrocatalysts for the oxygen evolution reaction, *ACS Catal.* 9(2), 1013 (2019)